

1 **“Anomalously weak Labrador Sea convection and Atlantic overturning during the past 150**  
2 **years”**

3 **David J.R. Thornalley<sup>1,2\*</sup>, Delia W. Oppo<sup>2</sup>, Pablo Ortega<sup>3</sup>, Jon I. Robson<sup>3</sup>, Chris M. Brierley<sup>1</sup>, Renee Davis<sup>1</sup>, Ian R.**  
4 **Hall<sup>4</sup>, Paola Moffa-Sanchez<sup>4</sup>, Neil L. Rose<sup>1</sup>, Peter T. Spooner<sup>1</sup>, Igor Yashayaev<sup>5</sup> & Lloyd D. Keigwin<sup>2</sup>**

5 *1) University College London, Department of Geography, UK*

6 *2) Woods Hole Oceanographic Institution, Department of Geology and Geophysics, USA*

7 *3) University of Reading, Department of Meteorology, Reading, U.K.*

8 *4) Cardiff University, School of Earth and Ocean Sciences, UK*

9 *5) Fisheries and Oceans Canada, Bedford Institute of Oceanography, Dartmouth, Canada*

10 \*To whom correspondence should be sent [d.thornalley@cantab.net](mailto:d.thornalley@cantab.net)

11

12 **The Atlantic meridional overturning circulation (AMOC) plays an essential role in climate**  
13 **through its redistribution of heat and its influence on the carbon cycle<sup>1,2</sup>. A recent decline in the**  
14 **AMOC may reflect decadal variability in Labrador Sea convection, but short observational**  
15 **datasets preclude a longer-term perspective on the modern state and variability of Labrador Sea**  
16 **convection and AMOC<sup>1,3-5</sup>. Here, we provide several lines of paleoceanographic evidence that**  
17 **Labrador Sea deep convection and AMOC have been anomalously weak over the past ~150 years**  
18 **(since the end of the Little Ice Age, LIA; ~1850 CE), in comparison to the preceding ~1500 years.**  
19 **The reconstructions suggest the transition occurred either as a predominantly abrupt shift**  
20 **around the end of the LIA, or, a more gradual, continued decline over the past 150 years; this**  
21 **ambiguity likely arises from additional non-AMOC influences on the proxies or their varying**  
22 **sensitivity to different components of the AMOC. We suggest that enhanced freshwater fluxes**  
23 **from the Arctic and Nordic Seas, towards the end of the LIA, sourced from melting glaciers and**  
24 **thickened sea-ice that had developed earlier in the LIA, weakened Labrador Sea convection and**  
25 **the AMOC. The lack of a subsequent recovery may result from hysteresis or twentieth century**  
26 **melting of the Greenland ice sheet<sup>6</sup>. Our results highlight that recent decadal variability of**

27 **Labrador Sea convection and the AMOC has occurred during an atypical, weak background**  
28 **state. Future work should aim to constrain the role of internal climate variability versus early**  
29 **anthropogenic forcing in the AMOC weakening described here.**

30 The AMOC is comprised of northward transport of warm surface and thermocline waters, and  
31 their deep southward return flow as dense waters that formed by cooling processes and sinking at high  
32 latitudes<sup>2</sup>. The stability of the AMOC in response to ongoing and projected climate change is uncertain.  
33 Monitoring of the AMOC by an array at 26°N, spanning the last decade, suggests a weakening of the  
34 AMOC, occurring ten times faster than expected from climate model projections<sup>1</sup>. However, it remains  
35 uncertain if this trend is part of a longer-term decline, natural multi-decadal variability, or a  
36 combination of both. Here, we develop past reconstructions of AMOC variability that can be directly  
37 compared to instrumental datasets and provide longer-term perspective.

38 The Labrador Sea is an important region for deep-water formation in the North Atlantic<sup>5</sup>.  
39 Moreover, modelling studies suggest that deep Labrador Sea density (dLSD) may be a useful predictor  
40 of AMOC change<sup>3,4,7</sup>. This is because density anomalies produced in the Labrador Sea - predominantly  
41 caused by varying deep convection - can propagate southwards rapidly (on the order of months) along  
42 the western margin via boundary waves, altering the cross-basin zonal density gradient, thus modifying  
43 geostrophic transport and therefore AMOC strength<sup>2-4,7-9</sup>. Building upon these studies, we show that  
44 dLSD anomalies are also associated with changes in the velocity of the deep western boundary current  
45 (DWBC) and the strength of the AMOC at 45°N in the high-resolution climate model HadGEM3-GC2  
46 (see Methods and Fig. 1).

47 In addition to this link between the AMOC and dLSD and the DWBC, changes in AMOC also  
48 alter ocean heat transport. Modeling studies suggest that AMOC weakening affects the upper ocean  
49 heat content of the eastern subpolar gyre (SPG) with a lag time of ~10 years (ref. <sup>10</sup>), and a distinct  
50 AMOC fingerprint on subsurface temperature (Tsub, 400m water depth)<sup>11</sup> characterizes weak AMOC  
51 phases, with a dipole pattern of warming of the Gulf Stream extension region<sup>12</sup> and cooling of the

52 subpolar Northeast Atlantic. We exploit the model-based covariance of decadal changes in AMOC with  
53 dLSD anomalies, SPG upper ocean heat content, and the Tsub fingerprint, to extend constraints on past  
54 AMOC variability (see Methods). Over the instrumental era (post ~1950), these indices suggest  
55 significant decadal variability in the AMOC, with coherent changes in dLSD, and lagged SPG upper  
56 ocean heat content and the Tsub AMOC fingerprint<sup>3,5,8,10,11</sup>.

57 The model results in Figure 1 imply that we can use flow speed reconstructions of the DWBC  
58 to infer past changes in dLSD and AMOC. We analyzed the sortable silt (SS) mean grain size, a proxy  
59 for near-bottom current flow speed<sup>13</sup>, in two marine sediment cores (48JPC and 56JPC; see Methods,  
60 Extended Data Fig. 1 and 2) located under the influence of southward flowing Labrador Sea Water  
61 (LSW) within the DWBC off Cape Hatteras (hereafter DWBC<sub>LSW</sub>). The high accumulation rates (~0.5-  
62 1 cm/yr) and modern core-top enable direct comparison of the record from 56JPC to observational  
63 datasets (Fig. 2).

64 In agreement with the model-predicted relationship (i.e. Fig. 1), changes in inferred flow speed  
65 of the DWBC<sub>LSW</sub> show similar, in-phase, variability with observed deep Labrador Sea density<sup>5</sup>.  
66 Moreover, there is strong covariability of our DWBC<sub>LSW</sub> proxy with the lagged (12 year) SPG upper  
67 ocean heat content and Tsub index from observational analysis (Fig. 2a). Over the past ~100 years, the  
68 spatial correlation of upper ocean heat content anomalies associated with our DWBC<sub>LSW</sub> proxy closely  
69 resembles the Tsub AMOC fingerprint (Fig. 2b,c), supporting the concept that the DWBC<sub>LSW</sub> proxy  
70 and upper ocean temperature changes provide complementary, coherent, information on a common  
71 phenomenon, namely AMOC variability. Combined, these datasets imply that decadal variability has  
72 been a dominant feature of the past 130 years, with the most recent strengthening of LSW formation  
73 during the mid-1990s, and the subsequent decline, being particularly prominent features.

74 To gain insight prior to the instrumental era, we first extend our DWBC<sub>LSW</sub> flow speed  
75 reconstruction (Fig. 3e). The DWBC<sub>LSW</sub> proxy suggests that AMOC has been weaker during the last  
76 ~150 years than at any other time during the last 1600 years. The emergence of this weaker state (i.e.

77 smoothed record exceeds a noise threshold of  $2\sigma$  pre-Industrial era variability), takes place at ~1880  
78 CE in both cores. The overall transition occurs from ~1750 to ~1900 CE, late in the Little Ice Age  
79 (LIA, ~1350-1850 CE) and the early stages of the Industrial era (defined as ~1830 onwards<sup>14</sup>).  
80 Applying the flow speed calibration for sortable silt<sup>13</sup> suggests a decrease from 17 to 14.5 cm/s at  
81 56JPC, and 14 to 12 cm/s at 48JPC, implying a decrease in DWBC<sub>LSW</sub> strength of ~15% (assuming  
82 constant DWBC<sub>LSW</sub> cross-sectional area). This decrease is equivalent to  $3\sigma$  and  $4\sigma$  of the pre-Industrial  
83 era variability in 48JPC and 56JPC, respectively.

84 Secondly, we compile quantitative proxy records of subsurface (~50-200m) ocean temperatures  
85 from key locations to extend the Tsub AMOC proxy (Fig. 3a-c; see Methods and Extended Data Fig. 3  
86 & 4). The Tsub proxy reconstruction provides support for the proposed AMOC weakening. Opposing  
87 temperature anomalies recorded in the two regions after ~1830 CE, with warming of the Gulf Stream  
88 extension region and cooling of the subpolar Northeast Atlantic, together suggest a weaker Industrial-  
89 era AMOC. Further support for the AMOC weakening is suggested by the spatial pattern of Tsub  
90 change in the Northwest Atlantic during the onset of the Industrial era (Extended Data Fig. 5). In  
91 contrast to the prominent changes recorded in our proxy reconstructions at the end of the LIA, more  
92 subdued variability occurs during the earlier part of our records (400-1800 CE). This implies that the  
93 forcing and AMOC response was weaker, or it supports mechanisms in which the AMOC does not play  
94 a leading role in the (multi-)centennial climate variability of this period<sup>15,16</sup>.

95 Labrador Sea deep convection is a major contributor to the AMOC, but susceptible to  
96 weakening<sup>5</sup>. Combined with its role in decadal variability over the last ~100 years (Fig. 2), and model  
97 analysis of mechanisms in operation today<sup>8</sup>, it is likely that changes in Labrador Sea convection were  
98 involved in the weakening of AMOC at the end of the LIA. Additional correlative (not necessarily  
99 causative) support is revealed by paleoceanographic evidence from the Labrador Sea. Strong deep  
100 convection in the Labrador Sea is typically associated with cooling and freshening of the subsurface

101 ocean<sup>5</sup>. Therefore, the reconstructed shift to warmer and saltier subsurface conditions in the northeast  
102 Labrador Sea<sup>17</sup> over the past ~150 years (Fig. 3d; equivalent to  $\sim 2\sigma$  of pre-Industrial era variability) is  
103 consistent with a shift to a state characterized by reduced deep convection, with only occasional  
104 episodes of sustained deep convection. Reconstructions of the other major deep-water contributors to  
105 the AMOC - the two Nordic Seas overflows - suggest that on centennial timescales they have varied in  
106 anti-phase and thus likely compensated for one another during the last 3000 years<sup>18</sup>. Hence, changes in  
107 Labrador Sea deep convection may have been the main cause of AMOC variability over this period.

108 While atmospheric circulation has played a dominant role in recent decadal variability of  
109 AMOC (and LSW)<sup>2,8</sup>, there is no strong evidence that the AMOC decrease at the end of the LIA was  
110 similarly caused by a shift in atmospheric circulation<sup>19</sup>. Instead, we hypothesize that the AMOC  
111 weakening was caused by enhanced freshwater fluxes associated with the melting and export of ice and  
112 freshwater from the Arctic and Nordic Seas. During the LIA, circum-Arctic glaciers and multi-year  
113 Arctic and Nordic sea ice were at their most advanced state of the last few thousand years, and there  
114 were large ice-shelves in the Canadian Arctic and exceptionally thick multi-year sea-ice. Yet, by the  
115 early 20<sup>th</sup> century, many of these features had disappeared or were retreating<sup>20-23</sup>.

116 Modelling studies suggest enhanced freshwater fluxes of  $\sim 10$ -100 mSv over a few decades can  
117 weaken Labrador Sea convection and AMOC<sup>24</sup>, although models with strong hysteresis of Labrador  
118 Sea convection<sup>25</sup> suggest this may be as little as 5-10 mSv. Unfortunately, there is little data to  
119 constrain the Arctic and Nordic Seas freshwater fluxes associated with the end of the LIA. The earliest  
120 observational datasets suggest  $\sim 10$  mSv from sea ice loss in the Arctic and Nordic Seas during 1895-  
121 1920<sup>26,27</sup>, to which we must also add melting of previously expanded circum-Arctic glaciers and ice-  
122 shelves, and enhanced melting of the Greenland ice-sheet (GIS). Alternatively, we can estimate that a 1  
123 m reduction in average Arctic sea-ice thickness during the termination of the LIA could yield a  
124 freshwater flux of 10 mSv for 50 years. While additional work is required to improve this incomplete

125 estimate, there was likely sufficient freshwater stored in the Arctic and Nordic Seas during the LIA to  
126 impact Labrador Sea convection and AMOC.

127 The AMOC weakening recorded in our two marine reconstructions is broadly similar to that in  
128 a predominantly terrestrial-based AMOC proxy reconstruction<sup>6</sup> (Fig. 3c). Our Tsub AMOC proxy and  
129 the AMOC proxy of ref. 6 (Fig. 3c), both suggest a substantial decline in AMOC through the 20<sup>th</sup>  
130 century, whereas our DWBC<sub>LSW</sub> AMOC proxy and the observational-based Tsub AMOC index (Fig.  
131 2a and Extended Data Fig. 6) suggest relatively little long-term AMOC decline during the 20<sup>th</sup> century.  
132 These differences may be attributed to several factors. Firstly, our sediment-core based Tsub proxy is  
133 subject to artificial smoothing, caused by combining numerous records with substantial (~10-100 year)  
134 individual age uncertainties, and compounded by bioturbation. Furthermore, the Tsub proxy sediment  
135 cores were retrieved in the late 1990s and early 2000s, therefore they cannot capture the strong Tsub  
136 index recovery from ~2000-2010 that reverses the earlier prolonged decline (see Extended Fig. 6).  
137 Alternatively, the earlier, more threshold-like change in the DWBC<sub>LSW</sub> AMOC proxy may be due to  
138 local shifts in the position of the DWBC, and/or non-linear dynamics of the DWBC response to AMOC  
139 change. However, based on the similarity of the DWBC<sub>LSW</sub> reconstructions from cores 56JPC and  
140 48JPC, located at different water depths, and the strong correlation of DWBC<sub>LSW</sub> with Labrador Sea  
141 density and the Tsub AMOC index over the instrumental period, we suggest these factors are not  
142 substantial. Finally, the differences between the AMOC reconstructions may reflect their varying  
143 response timescales and sensitivities to the different components of the AMOC and the SPG<sup>28,29</sup>.

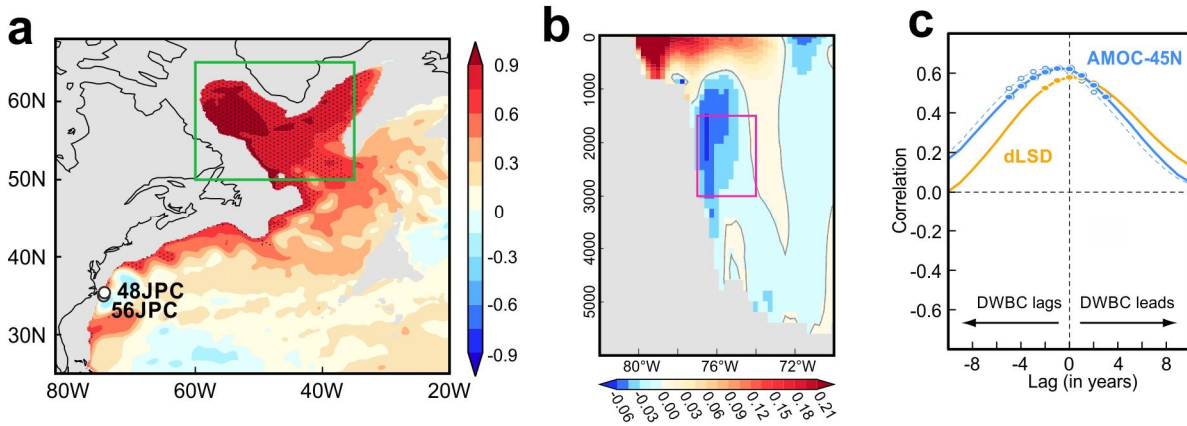
144 Our study raises several issues regarding the modelling of AMOC in historical experiments.  
145 The inferred transition to a weakened AMOC occurred near the onset of the Industrial-era, several  
146 decades before the strongest global warming trend, and has remained weak up to the present day. This  
147 either suggests hysteresis of the AMOC in response to an early climate forcing  $\delta$  natural (solar,  
148 volcanic) or anthropogenic (greenhouse gases, aerosols, land-use change) - or alternatively, continued  
149 climate forcing, such as the melting of the GIS<sup>6</sup>, has been sufficient to keep AMOC weak or cause

150 further weakening. Our reconstructions also differ from most climate model simulations, which show  
151 either negligible AMOC change or a later, more gradual reduction<sup>30</sup>. Many factors may be responsible  
152 for this model-data discrepancy: a misrepresentation of AMOC-related processes and possible  
153 hysteresis, including underestimation of AMOC sensitivity to climate (freshwater) forcing<sup>29,31</sup>; the  
154 underestimation or absence of important freshwater fluxes during the end of the LIA; and the lack of  
155 transient forced behaviour in the “constant forcing” pre-Industrial controls used to initialize historical  
156 forcings. Resolving these issues will be important for improving the accuracy of projected changes in  
157 AMOC.

158         In conclusion, our study reveals an anomalously weak AMOC over the last ~150 years. Because  
159 of its role in heat transport, it is often assumed that AMOC weakening cools the northern hemisphere.  
160 However, our study demonstrates that changes in AMOC are not always synchronous with temperature  
161 changes. That AMOC weakening occurred during the late LIA and onset of the Industrial era, rather  
162 than earlier in the LIA, may point to additional forcing factors at this time, such as an increase in the  
163 export of thickened Arctic and Nordic sea ice, or melting of circum-Arctic ice-shelves. The persistence  
164 of weak AMOC during the 20<sup>th</sup> century, when there was pronounced northern hemisphere and global  
165 warming, implies that other climate forcings, such as greenhouse gas warming, were dominant during  
166 this period. We therefore infer that AMOC has responded to recent centennial-scale climate change,  
167 rather than driven it. Regardless, the weak state of AMOC over the last ~150 years may have modified  
168 northward ocean heat transport, as well as atmospheric warming through altering ocean-atmosphere  
169 heat transfer<sup>32,33</sup>, underscoring the need for continued investigation of the role of the AMOC in climate  
170 change. Determining the future behaviour of AMOC will depend in part on constraining its sensitivity  
171 and possible hysteresis to freshwater input, for which improved historical estimates of these fluxes  
172 during the AMOC weakening reported here will be especially useful.

173

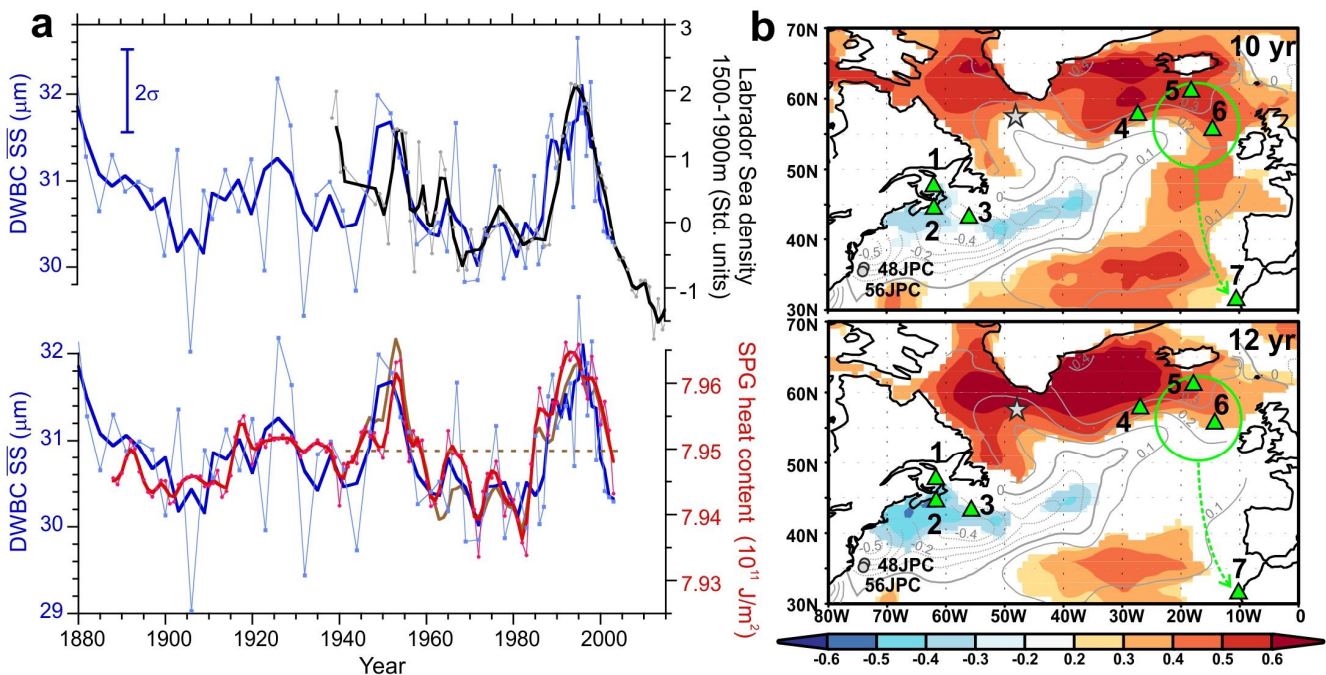
174



175

176 **Fig. 1. Modelled link of DWBC velocity with deep Labrador Sea density and AMOC.** **a**, Correlation of the  
 177 vertically-averaged ocean density (1000-2500m) with dLSD; green box, 1000-2500m average) in HadGEM3-  
 178 GC2 control run; cores sites for DWBC flow speed reconstruction shown. **b**, Climatology of the modelled  
 179 meridional ocean velocity ( $\text{ms}^{-1}$ ) 30-35°N (see Methods and Extended Data Fig. 7&8), illustrating the modelled  
 180 position of the DWBC. **c**, Cross-correlations between modelled averaged DWBC flow speed in pink box in **b**  
 181 and indices of dLSD and AMOC at 45°N (dashed line is without the Ekman component).

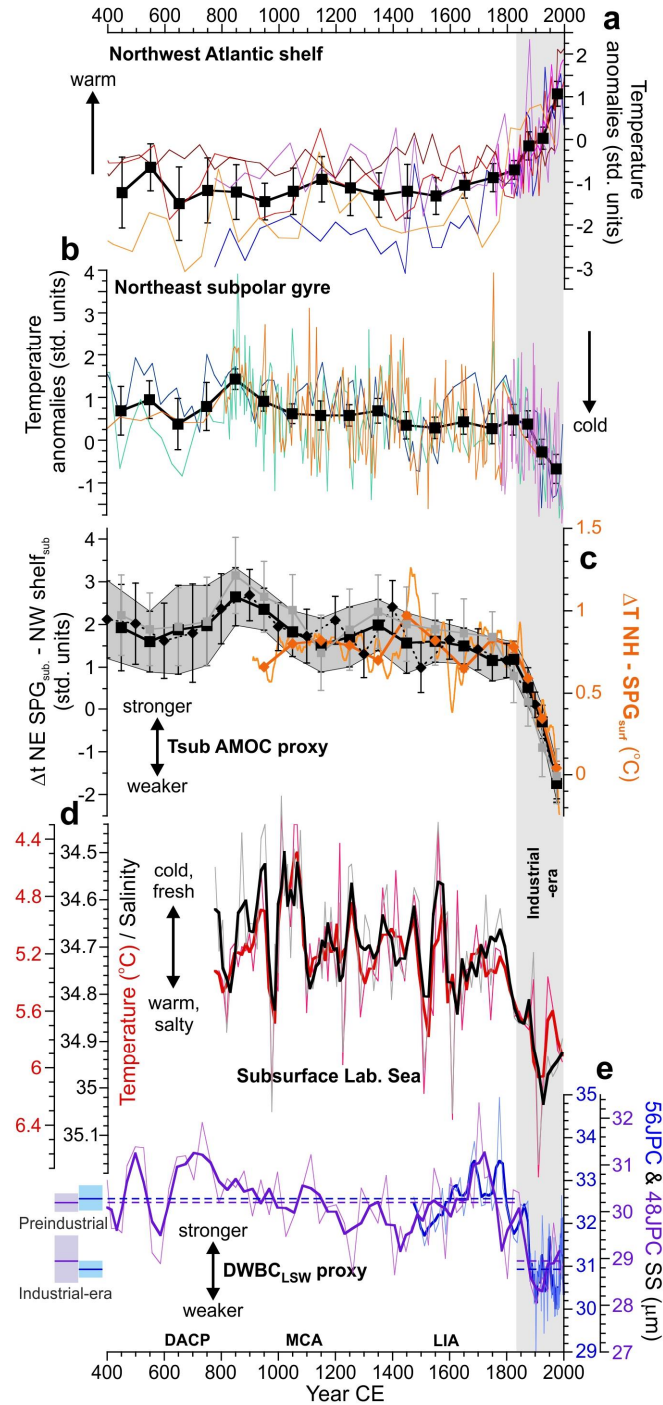
182



183

184 **Fig. 2. Proxy validation and recent, multi-decadal variability.** **a**, SS mean grain size (56JPC, blue) compared  
 185 with: central Labrador Sea annual density<sup>5</sup> (black;  $r^2=0.56$ ,  $n=54$ ), comparable to model-based dLSD (Extended  
 186 Data Fig. 9); and with 12-year lagged SPG upper ocean heat content (0-700m, 55-65°N, 15-60°W, EN4 dataset;  
 187 red;  $r^2=0.58$ ,  $n=116$ ) and Tsub AMOC fingerprint<sup>11</sup> (brown; dashed line zero-line;  $r^2=0.76$ ,  $n=55$ ). Correlations  
 188 (and  $2\sigma$  SS error bar,  $n=30$ ) are for 3-point means (bold). Low resolution 48JPC data not shown. **b**, 10- and 12-  
 189 yr lagged spatial correlation of upper ocean heat content (0-700m) with reconstructed DWBC<sub>LSW</sub> flow speed  
 190 (56JPC), heat content lags. Grey contours, spatial Tsub AMOC proxy<sup>11</sup>; green triangles, Tsub proxy sites; green  
 191 circle, surface region controlling benthic temperatures at site 7. Grey circles, DWBC sites; grey star, core site  
 192 ref. 17.

193



195

196 **Fig. 3. Proxy reconstructions of AMOC changes over the last 1600 years.** a,b, Subsurface Northwest Atlantic  
 197 shelf (a) and Northeast Atlantic subpolar gyre (b) temperatures; sites in Fig. 2b; composite stacks, black. c, Tsub  
 198 AMOC proxy (black, grey), various binning (see Extended Data Fig 4); orange, Rahmstorf AMOC proxy<sup>6</sup>, 1°C =  
 199 ~2.3Sv, 21-yr smooth, thin line; thick line and symbols, binned as for Tsub AMOC proxy. d, *N. pachyderma*  
 200 Mg/Ca- $\delta^{18}\text{O}$  subsurface (~100-200m) temperature and salinity for northeast Labrador Sea<sup>17</sup>. e, SS mean grain  
 201 size (56JPC, blue; 48JPC, purple; bold, 3-point means); dashed lines, Industrial/Preindustrial-era averages. Error  
 202 bars/shading,  $\pm 2\text{SE}$ . DACP (Dark Ages Cold Period, ~400-800 CE), MCA (Medieval Climate Anomaly, ~900-  
 203 1250 CE).

204 **References**

- 205 1. Srokosz, M. A. & Bryden, H. L. Observing the Atlantic Meridional Overturning Circulation yields  
206 a decade of inevitable surprises. *Science* 348, doi:10.1126/science.1255575 (2015).
- 207 2. Buckley, M. W. & Marshall, J. Observations, inferences, and mechanisms of the Atlantic  
208 Meridional Overturning Circulation: A review. *Reviews of Geophysics* 54, 5-63,  
209 doi:10.1002/2015RG000493 (2016).
- 210 3. Jackson, L. C., Peterson, K. A., Roberts, C. D. & Wood, R. A. Recent slowing of Atlantic  
211 overturning circulation as a recovery from earlier strengthening. *Nature Geosci* 9, 518-522,  
212 doi:10.1038/ngeo2715 (2016).
- 213 4. Robson, J., Hodson, D., Hawkins, E. & Sutton, R. Atlantic overturning in decline? *Nature Geosci*  
214 7, 2-3, doi:10.1038/ngeo2050 (2014).
- 215 5. Yashayaev, I. Hydrographic changes in the Labrador Sea, 1960-2005. *Progress in Oceanography*  
216 73, 242-276, doi: 10.1016/j.pocean.2007.04.015 (2007).
- 217 6. Rahmstorf, S. et al. Exceptional twentieth-century slowdown in Atlantic Ocean overturning  
218 circulation. *Nature Clim. Change* 5, 475-480, doi:10.1038/nclimate2554 (2015).
- 219 7. Hodson, D. L. R. & Sutton, R. T. The impact of resolution on the adjustment and decadal  
220 variability of the Atlantic meridional overturning circulation in a coupled climate model. *Climate*  
221 *Dynamics* 39, 3057-3073, doi:10.1007/s00382-012-1309-0 (2012).
- 222 8. Ortega, P., Robson, J., Sutton, R. T. & Andrews, M. B. Mechanisms of decadal variability in the  
223 Labrador Sea and the wider North Atlantic in a high-resolution climate model. *Climate Dynamics*,  
224 doi:10.1007/s00382-016-3467-y (2016).
- 225 9. Roberts, C. D., Garry, F. K. & Jackson, L. C. A Multimodel Study of Sea Surface Temperature and  
226 Subsurface Density Fingerprints of the Atlantic Meridional Overturning Circulation. *Journal of*  
227 *Climate* 26, 9155-9174, doi:10.1175/jcli-d-12-00762.1 (2013).
- 228 10. Robson, J., Ortega, P. & Sutton, R. A reversal of climatic trends in the North Atlantic since 2005.  
229 *Nature Geosci* 9, 513-517, doi:10.1038/ngeo2727 (2016).
- 230 11. Zhang, R. Coherent surface-subsurface fingerprint of the Atlantic meridional overturning  
231 circulation. *Geophysical Research Letters* 35, doi:10.1029/2008GL035463 (2008).
- 232 12. Saba, V. S. et al. Enhanced warming of the Northwest Atlantic Ocean under climate change.  
233 *Journal of Geophysical Research: Oceans* 121, 118-132, doi:10.1002/2015JC011346 (2016).
- 234 13. McCave, I. N., Thornalley, D. J. R. & Hall, I. R. Relation of sortable silt grain-size to deep-sea  
235 current speeds: Calibration of the Mud Current Meter. *Deep Sea Research Part I: Oceanographic*  
236 *Research Papers*, doi:10.1016/j.dsr.2017.07.003 (2017).
- 237 14. Abram, N. J. et al. Early onset of industrial-era warming across the oceans and continents. *Nature*  
238 536, 411-418, doi:10.1038/nature19082 (2016).

- 239 15. Moreno-Chamarro, E., Zanchettin, D., Lohmann, K. & Jungclaus, J. H. An abrupt weakening of  
240 the subpolar gyre as trigger of Little Ice Age-type episodes. *Climate Dynamics* 48, 727-744,  
241 doi:10.1007/s00382-016-3106-7 (2017).
- 242 16. Miller, G. H. et al. Abrupt onset of the Little Ice Age triggered by volcanism and sustained by sea-  
243 ice/ocean feedbacks. *Geophysical Research Letters* 39, doi:10.1029/2011gl050168 (2012).
- 244 17. Moffa-Sánchez, P., Hall, I. R., Barker, S., Thornalley, D. J. R. & Yashayaev, I. Surface changes in  
245 the eastern Labrador Sea around the onset of the Little Ice Age. *Paleoceanography* 29, 160-175,  
246 doi:10.1002/2013PA002523 (2014).
- 247 18. Moffa-Sanchez, P., Hall, I. R., Thornalley, D. J. R., Barker, S. & Stewart, C. Changes in the  
248 strength of the Nordic Seas Overflows over the past 3000 years. *Quaternary Science Reviews* 123,  
249 134-143, doi: 10.1016/j.quascirev.2015.06.007 (2015).
- 250 19. Ortega, P. et al. A model-tested North Atlantic Oscillation reconstruction for the past millennium.  
251 *Nature* 523, 71-74, doi:10.1038/nature14518 (2015).
- 252 20. Bradley, R. S. & England, J. H. The Younger Dryas and the Sea of ancient ice. *Quaternary*  
253 *Research* 70, 1-10 (2008).
- 254 21. Funder, S. et al. A 10,000-Year Record of Arctic Ocean Sea-Ice Variability View from the  
255 Beach. *Science* 333, 747-750, doi:10.1126/science.1202760 (2011).
- 256 22. Vincent, W. F., Gibson, J. A. E. & Jeffries, M. O. Ice-shelf collapse, climate change, and habitat  
257 loss in the Canadian high Arctic. *Polar Record* 37, 133-142, doi:10.1017/S0032247400026954  
258 (2001).
- 259 23. Cabedo-Sanz, P., Belt, S. T., Jennings, A. E., Andrews, J. T. & Geirsdóttir, Á. Variability in drift  
260 ice export from the Arctic Ocean to the North Icelandic Shelf over the last 8000 years: A multi-  
261 proxy evaluation. *Quaternary Science Reviews* 146, 99-115,  
262 doi:http://dx.doi.org/10.1016/j.quascirev.2016.06.012 (2016).
- 263 24. Yang, Q. et al. Recent increases in Arctic freshwater flux affects Labrador Sea convection and  
264 Atlantic overturning circulation. *7*, 10525, doi:10.1038/ncomms10525 (2016).
- 265 25. Schulz, M., Prange, M. & Klocker, A. Low-frequency oscillations of the Atlantic Ocean  
266 meridional overturning circulation in a coupled climate model. *Climate of the Past* 3, 97-107  
267 (2007).
- 268 26. Polyakov, I. V. et al. Arctic Ocean Freshwater Changes over the Past 100 Years and Their Causes.  
269 *Journal of Climate* 21, 364-384, doi:10.1175/2007jcli1748.1 (2008).
- 270 27. Vinje, T. Anomalies and Trends of Sea-Ice Extent and Atmospheric Circulation in the Nordic Seas  
271 during the Period 1864-1998. *Journal of Climate* 14, 255-267, doi:10.1175/1520-  
272 0442(2001)014<0255:aatosi>2.0.co;2 (2001).
- 273 28. Drijfhout, S., Oldenborgh, G. J. v. & Cimadoribus, A. Is a Decline of AMOC Causing the Warming  
274 Hole above the North Atlantic in Observed and Modeled Warming Patterns? *Journal of Climate*  
275 25, 8373-8379, doi:10.1175/jcli-d-12-00490.1 (2012).

- 276 29. Sgubin, G., Swingedouw, D., Drijfhout, S., Mary, Y. & Bennabi, A. Abrupt cooling over the North  
277 Atlantic in modern climate models. 8, doi:10.1038/ncomms14375 (2017).
- 278 30. Weaver, A. J. et al. Stability of the Atlantic meridional overturning circulation: A model  
279 intercomparison. *Geophysical Research Letters* 39, doi:10.1029/2012gl053763 (2012).
- 280 31. Liu, W., Xie, S.-P., Liu, Z. & Zhu, J. Overlooked possibility of a collapsed Atlantic Meridional  
281 Overturning Circulation in warming climate. *Science Advances* 3, doi:10.1126/sciadv.1601666  
282 (2017).
- 283 32. Drijfhout, S. Competition between global warming and an abrupt collapse of the AMOC in Earth's  
284 energy imbalance. *Scientific Reports* 5, 14877, doi:10.1038/srep14877 (2015).
- 285 33. Kostov, Y., Armour, K. C. & Marshall, J. Impact of the Atlantic meridional overturning circulation  
286 on ocean heat storage and transient climate change. *Geophysical Research Letters* 41, 2108-2116,  
287 doi:10.1002/2013GL058998 (2014).

288

## 289 **Acknowledgements**

290 We thank Ellen Roosen for help with core sampling, Henry Abrams, Sean O'Keefe, Kathryn Pietro,  
291 Lindsey Owen and Francesco Pallottino for assistance in processing sediment samples; Kitty Green for  
292 faunal counts in 10MC; Martin Andrews at the UK Met Office for providing the model data; and  
293 Stefan Rahmstorf for useful suggestions. Funding was provided by NSF grant OCE-1304291 to DO,  
294 DT, LK; NERC Project DYNAMOC (NE/M005127/1) to PO and JR; NERC LTSM ACSIS to JR; by  
295 the Leverhulme Trust and ATLAS to DT. This project has received funding from the European Union's  
296 Horizon 2020 research and innovation programme under grant agreement No 678760 (ATLAS). This  
297 output reflects only the authors' views and the European Union cannot be held responsible for any use  
298 that may be made of the information contained therein.

299

## 300 **Author contributions**

301 Conceived by DT; NSF project proposal written and managed by DO and DT; cores 56JPC and 48JPC  
302 collected by LK; SS analysis and interpretation by DT, with contributions from PS and RD; modelling

303 work by PO and JR; SCP analysis by NR; Monte-Carlo modeling by PS; first draft written by DT; all  
304 authors contributed to discussion and final version of the manuscript.

305

## 306 **Author Information**

307 The authors declare no competing financial interests.

308 Reprints and permissions information is available at [www.nature.com/reprints](http://www.nature.com/reprints).

309 Correspondence and requests for materials should be addressed to [d.thornalley@cantab.net](mailto:d.thornalley@cantab.net)

310

## 311 **METHODS**

### 312 **Climate model investigation of AMOC and DWBC changes**

313 The climate model used in this study was the UK Met Office's Third Hadley Centre Global  
314 Environmental Model ó Global Coupled Configuration two (HadGEM3óGC2). The ocean model for  
315 HadGEM3-GC2 is the Global Ocean version 5.0, which is based on the version 3.4 of the Nucleus for  
316 European Models of the Ocean model (NEMO)<sup>34</sup>. The ocean model has 75 vertical levels, and is run at  
317 a nominal ¼° resolution using the NEMO tri-polar grid. The atmospheric component is the Global  
318 Atmosphere version 6.0 of the UK Met Office Unified Model, and is run at N216 resolution (~60km in  
319 mid-latitudes), with 85 vertical levels. More information on the model can be found in Williams et al<sup>35</sup>.  
320 The experiment analyzed here was a 310-year control simulation of HadGEM3-GC2, i.e. it includes no  
321 changes in external forcings. This experiment was previously run and analyzed in Ortega et al<sup>8</sup>, where  
322 details of the specific model experiment are included. This coupled simulation has a relatively high  
323 spatial resolution for a more accurate representation of the boundary currents, and is sufficiently long to  
324 resolve a large number of decadal oscillations. All model data has been linearly detrended to remove  
325 any potential drift, and smoothed with a 10-year running mean in order to focus on the decadal and  
326 multi-decadal variability.

327 We use the model-based relationships to support the interpretation of the proxy-based AMOC  
328 reconstructions, which cannot be validated with the limited observations available. The AMOC at 45°N  
329 is chosen as this is the latitude with the largest correlations with both the deep Labrador Sea Density  
330 (dLSD) and deep western boundary current (DWBC) velocity index in the model. Note that AMOC  
331 indices defined at other latitudes (e.g. 35°N, 40°N) produce weaker, but still significant correlations  
332 with both dLSD and the DWBC. The simulated DWBC velocity index is the average of 30-35°N as at  
333 35°N (the latitude where the sediment cores were taken) the DWBC is found offshore, which we  
334 believe is associated with the model's Gulf Stream separating further north than in the observations  
335 (Extended Data Fig. 7). It should be noted, however, that changes in the position of the observed Gulf  
336 Stream do not appear to directly control the reconstructed flow speed changes in the DWBC<sub>LSW</sub> (see  
337 Extended Data Fig. 10).

338 We have also assessed the robustness of the model-based relationships to the smoothing. For  
339 example we reproduced the cross-correlation analysis in Fig. 1c using undetrended and/or unsmoothed  
340 data instead. In all cases, the lead-lags relationships are similar, with larger correlations emerging when  
341 the decadal smoothing is applied. Furthermore, we also tested the sensitivity of the model-based  
342 relationships to the specific model used. In particular, we repeated the analysis of Fig. 1 in the 340 year  
343 control experiment using the HiGEM climate model<sup>36</sup>. HiGEM has a similar horizontal ocean  
344 resolution (1/3°), but is based on a different ocean model. Encouragingly, Extended Data Fig. 8 shows  
345 that the results are consistent across the two models, in particular the link between dLSD and the  
346 DWBC, and between the DWBC and the AMOC at 45°N. However, there are some caveats. For  
347 example, both models' Gulfstream separate too far north, which led us to define the DWBC flow  
348 indices slightly south of the core sites. HiGEM also has a deeper DWBC than HadGEM3-GC2.  
349 Therefore, the DWBC index was computed at different levels in both models in order to represent the  
350 link between dLSD and the DWBCs. However, despite these differences, both models support the

351 general interpretation that the DWBC in the vicinity of Cape Hatteras is strongly connected with  
352 changes in the dLSD and the AMOC.

353 The interpretation of the model results is consistent with previously published model studies  
354 (both low and high resolution) that have revealed a coupling between the AMOC and/or Labrador Sea  
355 density, and the DWBC<sup>3,7,11,37</sup>. These modelled relationships support a causal link for the correlations  
356 between the instrumental records of Labrador Sea density and the reconstructed DWBC velocity,  
357 presented in Fig 2. Furthermore, recent instrumental data of the DWBC at 39°N spanning 2004-2014  
358 reveal that a reduction in the velocity of classical LSW within the DWBC is also accompanied by a  
359 decrease in its density<sup>38</sup>, as hypothesized here. The observed decrease in the velocity and density of  
360 classical LSW within the DWBC between 2004 and 2014 is also consistent with the decrease in the  
361 density of the deep Labrador Sea over this period (Fig. 2a and Extended Data Fig. 9), although a longer  
362 observational DWBC time-series is needed to gain confidence in this relationship.

363

#### 364 **Age models**

365 New and updated age models for the cores are presented in Extended Figures 1 & 2, and are based on  
366 <sup>14</sup>C, <sup>210</sup>Pb and spheroidal carbonaceous particle (SCP) concentration profiles<sup>39</sup>.

367

#### 368 **Sortable silt data**

369 Two marine sediment cores were used for DWBC flow speed reconstruction: KNR-178-56JPC  
370 (~35°28'N, 74°43'W, 1718 m water depth) and KNR-178-48JPC (35°46'N, 74°27'W, 2009 m water  
371 depth). Sediments were processed using established methods<sup>40</sup> taking 1cm wide samples, every 1cm for  
372 the top 63cm and then every 4cm down to 200cm in 56JPC, and every 1cm down to 71cm in 48JPC.  
373 Samples were analyzed at Cardiff University on a Beckman Coulter Multisizer 4 using the Enhanced  
374 Performance Multisizer 4 beaker and stirrer setting 30 to ensure full sediment suspension. Two or three  
375 separate aliquots were analyzed for each sample, sizing 70,000 particles per aliquot. Analytical

376 precision was ~1% ( $\pm 0.3$  m), whilst full procedural error (based on replicates of ~25% of samples,  
377 starting from newly sampled bulk sediment) was  $\pm 0.8$  m.

378

### 379 **Temperature data and constructing the Tsub index**

380 Numerous studies have suggested AMOC variability is associated with a distinct surface or subsurface  
381 (400m) temperature fingerprint in the North Atlantic<sup>6,11,28,41</sup>. However, the lack of long-term  
382 observations of AMOC prevents accurate diagnosis of the precise AMOC temperature fingerprint, and  
383 models display a range of different AMOC temperature fingerprints<sup>9,42</sup>. In this study we focus on the  
384 Tsub AMOC fingerprint, proposed by Zhang<sup>11</sup> on the basis of covariance between modelled AMOC,  
385 the spatial pattern of the leading mode of subsurface (400m) temperature variability, and sea-surface  
386 height changes. These model-based relationships were supported by similar relationships (spatial and  
387 temporal) observed in recent instrumental data of subsurface temperature and sea surface height. The  
388 agreement between our DWBC<sub>LSW</sub> AMOC reconstruction, observed Labrador Sea density changes, and  
389 the Tsub AMOC fingerprint, provides support for our approach and suggests the Tsub AMOC  
390 fingerprint is capturing an important component of deep AMOC variability. Differences between the  
391 various proposed AMOC temperature fingerprints likely reflects their sensitivity to different aspects of  
392 AMOC and heat transport in the North Atlantic e.g. AMOC versus SPG circulation<sup>28</sup>; the temperature  
393 response to each of these components may be resolved if more comprehensive spatial networks of past  
394 North Atlantic temperature variability are generated<sup>43</sup>.

395       Records used in the OCEAN 2K synthesis<sup>44</sup> from the Northwest Atlantic slope and the subpolar  
396 Northeast Atlantic were selected and supplemented with additional records that also record past  
397 temperature variability in the subsurface ocean of the chosen region. Cores that did not have a modern  
398 core top age (1950 CE or younger) or resolution of better than 100 years were not included.  
399 Foraminiferal-based temperature proxies were selected because they record subsurface temperatures  
400 (typically 50-200m), upon which the Tsub proxy is based. We avoid other temperature proxies (e.g.

401 alkenones, coccolithores, diatoms) that are typically more sensitive to sea surface temperature, rather  
402 than Tsub, and which also use the fine fraction that at the drift sites required for the necessary age  
403 resolution contains significant allochthonous material, compromising the fidelity of *in situ* temperature  
404 reconstruction<sup>45,46</sup>.

405 All Tsub records were normalized to the interval 1750-2000 CE (the length of the shortest  
406 records). The Tsub proxy reconstruction was calculated as the difference between the stacked  
407 temperature records of the Northwest and Northeast Atlantic. Our results are insensitive to the precise  
408 binning or stacking method, as shown in Extended Data Fig. 4. The sedimentation rates of the cores  
409 used, combined with the effects of bioturbation mean we cannot resolve signals on timescales shorter  
410 than ~20-50 years. Age model uncertainty is estimated to be up to ~30 years for the last ~150 years  
411 where cores have <sup>210</sup>Pb dating, and ~100 years for 400-1800 CE where <sup>14</sup>C dating is relied upon.  
412 Therefore, the optimal bin intervals chosen were 50 years for 1800-2000 CE, and 100 years for 400-  
413 1800 CE. Results for only using 50 year and 100 year bins, as well as 30 year bins for the top 200  
414 years, are shown in Extended Data Fig. 4.

415

#### 416 **Data Availability**

417 The proxy data that support these findings are provided with the paper as Source Data for Fig. 2, 3,  
418 Extended Data Fig 1, 2, 4, 5, 6, 9, and at NGDC Paleoclimatology ([https://www.ncdc.noaa.gov/data-  
419 access/paleoclimatology-data/datasets](https://www.ncdc.noaa.gov/data-access/paleoclimatology-data/datasets)). Model data can be made available from Jon Robson  
420 ([j.i.robson@reading.ac.uk](mailto:j.i.robson@reading.ac.uk)) upon reasonable request.

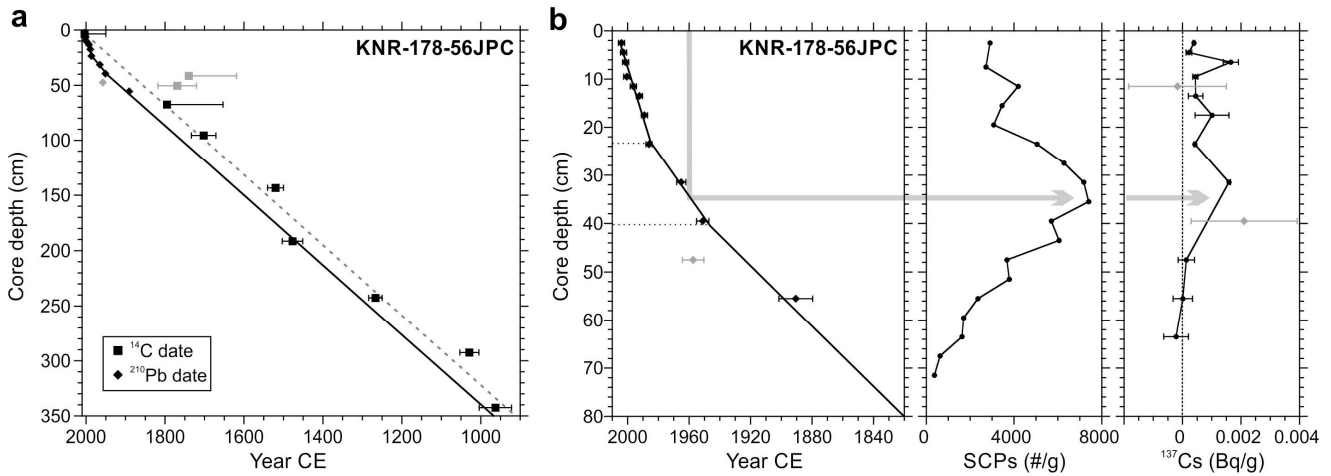
421

422 **References**

- 423 34. Megann, A. et al. GO5.0: the joint NERC&Met Office NEMO global ocean model for use in  
424 coupled and forced applications. *Geosci. Model Dev.* 7, 1069-1092, doi:10.5194/gmd-7-1069-2014  
425 (2014).
- 426 35. Williams, K. D. et al. The Met Office Global Coupled model 2.0 (GC2) configuration. *Geosci.*  
427 *Model Dev.* 8, 1509-1524, doi:10.5194/gmd-8-1509-2015 (2015).
- 428 36. Shaffrey, L. C. et al. U.K. HiGEM: The New U.K. High-Resolution Global Environment Model  
429 Model Description and Basic Evaluation. *Journal of Climate* 22, 1861-1896,  
430 doi:10.1175/2008jcli2508.1 (2009).
- 431 37. Bakker, P., Govin, A., Thornalley, D. J. R., Roche, D. M. & Renssen, H. The evolution of deep-  
432 ocean flow speeds and 13C under large changes in the Atlantic overturning circulation: Toward a  
433 more direct model-data comparison. *Paleoceanography* 30, 95-117, doi:10.1002/2015PA002776  
434 (2015).
- 435 38. Toole, J. M., Andres, M., Le Bras, I. A., Joyce, T. M. & McCartney, M. S. Moored observations of  
436 the Deep Western Boundary Current in the NW Atlantic: 2004&2014. *Journal of Geophysical*  
437 *Research: Oceans* 122, 7488-7505, doi:10.1002/2017JC012984 (2017).
- 438 39. Rose, N. L. Spheroidal Carbonaceous Fly Ash Particles Provide a Globally Synchronous  
439 Stratigraphic Marker for the Anthropocene. *Environmental Science & Technology* 49, 4155-4162,  
440 doi:10.1021/acs.est.5b00543 (2015).
- 441 40. McCave, I. N., Manighetti, B., Robinson, S.G. Sortable silt and fine sediment size/composition  
442 slicing: Parameters for palaeocurrent speed and palaeoceanography. *Paleoceanography* 10, 593-  
443 610 (1995).
- 444 41. Dima, M. & Lohmann, G. Evidence for Two Distinct Modes of Large-Scale Ocean Circulation  
445 Changes over the Last Century. *Journal of Climate* 23, 5-16, doi:10.1175/2009jcli2867.1 (2010).
- 446 42. Muir, L. C. & Fedorov, A. V. How the AMOC affects ocean temperatures on decadal to centennial  
447 timescales: the North Atlantic versus an interhemispheric seesaw. *Climate Dynamics* 45, 151-160,  
448 doi:10.1007/s00382-014-2443-7 (2015).
- 449 43. Ortega, P., Robson, J., Moffa-Sanchez, P., Thornalley, D. J. R. & Swingedouw, D. A last  
450 millennium perspective on North Atlantic variability: exploiting synergies between models and  
451 proxy data. *CLIVAR exchanges* 72, 61-67, doi:10.22498/pages.25.1 (2017).
- 452 44. McGregor, H. V. et al. Robust global ocean cooling trend for the pre-industrial Common Era.  
453 *Nature Geosci* 8, 671-677, doi:10.1038/ngeo2510 (2015).
- 454 45. McCave, I. N. A Poisoned Chalice? *Science* 298, 1186-1187, doi:10.1126/science.1076960 (2002).
- 455 46. Filippova, A., Kienast, M., Frank, M. & Schneider, R. R. Alkenone paleothermometry in the North  
456 Atlantic: A review and synthesis of surface sediment data and calibrations. *Geochemistry,*  
457 *Geophysics, Geosystems* 17, 1370-1382, doi:10.1002/2015GC006106 (2016).

- 458 47. Marchitto, T. & deMenocal, P. Late Holocene variability of upper North Atlantic Deep Water  
459 temperature and salinity. *Geochemistry Geophysics Geosystems* 4, 1100,  
460 doi:1110.1029/2003GC000598 (2003).
- 461 48. Keigwin, L. D., Sachs, J. P. & Rosenthal, Y. A 1600-year history of the Labrador Current off Nova  
462 Scotia. *Climate Dynamics* 21, 53-62, doi:10.1007/s00382-003-0316-6 (2003).
- 463 49. Keigwin, L. D. & Pickart, R. S. Slope Water Current over the Laurentian Fan on Interannual to  
464 Millennial Time Scales. *Science* 286, 520-523, doi:10.1126/science.286.5439.520 (1999).
- 465 50. Genovesi, L. et al. Recent changes in bottom water oxygenation and temperature in the Gulf of St.  
466 Lawrence: Micropaleontological and geochemical evidence. *Limnology and Oceanography* 56,  
467 1319-1329, doi:10.4319/lo.2011.56.4.1319 (2011).
- 468 51. Hall, I. R., Boessenkool, K. P., Barker, S., McCave, I. N. & Elderfield, H. Surface and deep ocean  
469 coupling in the subpolar North Atlantic during the last 230 years. *Paleoceanography* 25, n/a-n/a,  
470 doi:10.1029/2009PA001886 (2010).
- 471 52. Moffa-Sanchez, P., Born, A., Hall, I. R., Thornalley, D. J. R. & Barker, S. Solar forcing of North  
472 Atlantic surface temperature and salinity over the past millennium. *Nature Geosci* 7, 275-278,  
473 doi:10.1038/ngeo2094 (2014).
- 474 53. Thornalley, D. J. R., Elderfield, H. & McCave, I. N. Holocene oscillations in temperature and  
475 salinity of the surface subpolar North Atlantic. *Nature* 457, 711-714, doi:10.1038/nature07717  
476 (2009).
- 477 54. Richter, T. O., Peeters, F. J. C. & van Weering, T. C. E. Late Holocene (0-2.4 ka BP) surface water  
478 temperature and salinity variability, Feni Drift, NE Atlantic Ocean. *Quaternary Science Reviews*  
479 28, 1941-1955, doi:10.1016/j.quascirev.2009.04.008 (2009).
- 480 55. Morley, A. et al. Solar modulation of North Atlantic central Water formation at multidecadal  
481 timescales during the late Holocene. *Earth and Planetary Science Letters* 308, 161-171,  
482 doi:10.1016/j.epsl.2011.05.043 (2011).
- 483 56. Morley, A., Rosenthal, Y. & deMenocal, P. Ocean-atmosphere climate shift during the mid-to-late  
484 Holocene transition. *Earth and Planetary Science Letters* 388, 18-26, doi:  
485 10.1016/j.epsl.2013.11.039 (2014).
- 486 57. Sicre, M.-A. et al. A 4500-year reconstruction of sea surface temperature variability at decadal  
487 time-scales off North Iceland. *Quaternary Science Reviews* 27, 2041-2047,  
488 doi:10.1016/j.quascirev.2008.08.009 (2008).
- 489 58. Joyce, T. M. & Zhang, R. On the Path of the Gulf Stream and the Atlantic Meridional Overturning  
490 Circulation. *Journal of Climate* 23, 3146-3154, doi:10.1175/2010jcli3310.1 (2010).
- 491 59. Suman, D. O. & Bacon, M. P. Variations in Holocene sedimentation in the North American Basin  
492 determined from 230Th measurements. *Deep Sea Research Part A. Oceanographic Research*  
493 *Papers* 36, 869-878, doi: 10.1016/0198-0149(89)90033-2 (1989).

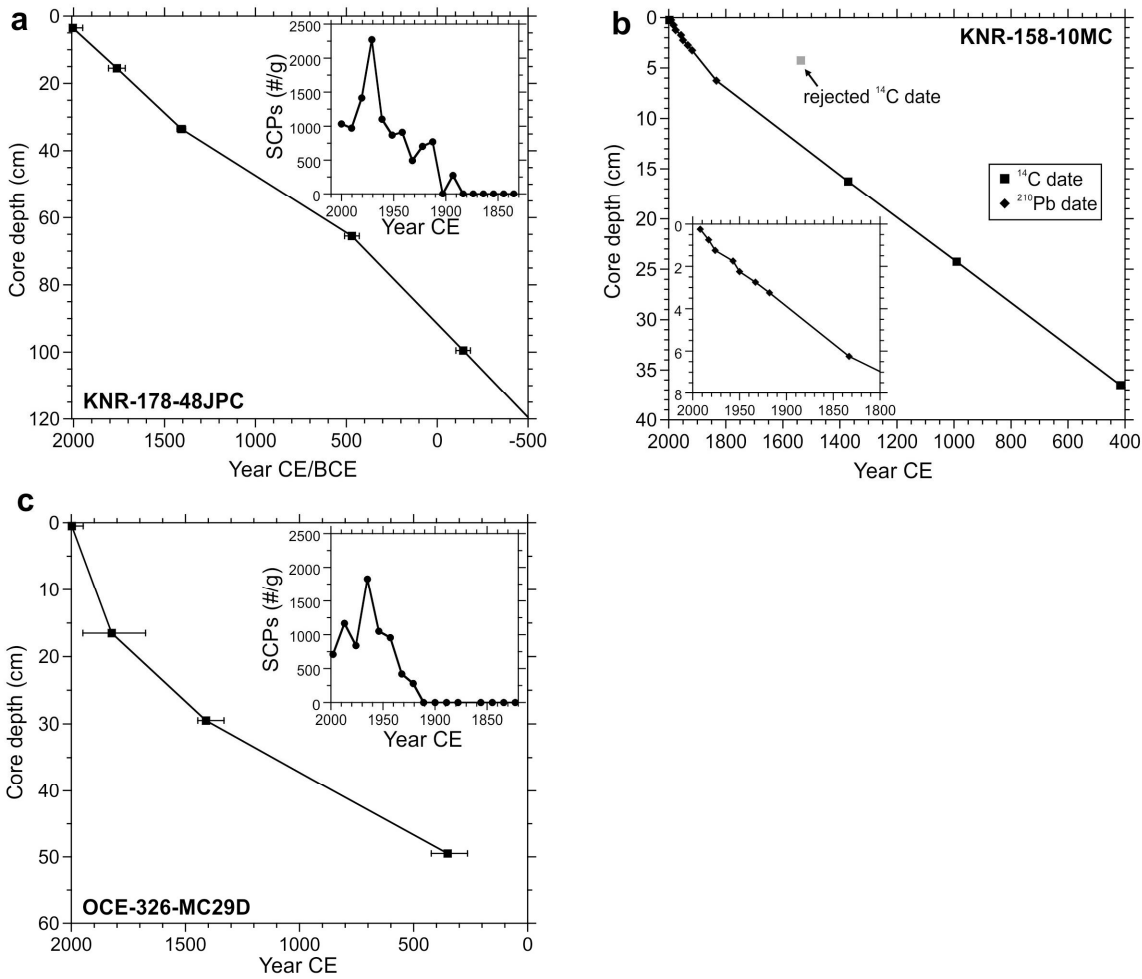
- 494 560. Adkins, J. F., Boyle, E. A., Keigwin, L. & Cortijo, E. Variability of the North Atlantic  
495 thermohaline circulation during the last interglacial period. *Nature* 390, 154-156,  
496 doi:10.1038/36540 (1997).
- 497 61. Hodson, D. L. R., Robson, J. I. & Sutton, R. T. An Anatomy of the Cooling of the North Atlantic  
498 Ocean in the 1960s and 1970s. *Journal of Climate* 27, 8229-8243, doi:10.1175/jcli-d-14-00301.1  
499 (2014).
- 500



501  
502

503 **Extended Data Figure 1. Age model for core KNR-178-56JPC.** a,  $^{14}\text{C}$  and  $^{210}\text{Pb}$  dating.  $^{14}\text{C}$  ages (with  $1\sigma$   
504 ranges; grey, rejected dates) on planktonic foraminifera yielded a modern core top age and indicate an average  
505 sedimentation rate over the last 1000 years of 320cm/kyr (dashed line). The presence throughout the core of  
506 abundant lithogenic grains in the >150 m fraction, alongside the coarse sortable silt mean grain size values,  
507 suggest some reworking of foraminifera is likely, resulting in average  $^{14}\text{C}$  ages that may be slightly (~50 years)  
508 older than their final depositional age, consistent with the  $^{210}\text{Pb}$  dates not splicing smoothly into the  $^{14}\text{C}$  ages ( $^{14}\text{C}$   
509 ages appear slightly too old). The final age model was therefore based on the  $^{210}\text{Pb}$  ages for the last century, and  
510 was then simply extrapolated back in time using the linear sedimentation rate of 320cm/kyr. Given that none of  
511 our findings are dependent on close age control in the older section of this core (i.e. pre 1880 CE), this  
512 uncertainty (converted  $^{14}\text{C}$  ages are ~50 years older than the extrapolated linear age model) does not affect the  
513 conclusions of our study. b, The age model for the top 80cm of 56JPC is based on  $^{210}\text{Pb}$  dating of bulk sediment  
514 assuming the constant initial concentration (CIC) method (rejecting the date at 47cm ó likely burrow). A simple  
515 two-segment linear fit to the  $^{210}\text{Pb}$  dates was adopted (rather than point-to-point interpolation or a spline)  
516 because sedimentological evidence - an abrupt increase in the % coarse fraction at 23cm depth, not observed  
517 elsewhere in the core, is indicative of a step change in the sedimentation rate. Further support for the age model  
518 of 56JPC over the last century is derived from the down-core abundance profile of spheroidal carbonaceous  
519 particles (SCPs, derived from high temperature fossil fuel combustion, counted using the methods described in  
520 ref. <sup>39</sup>) which ramped up from the mid-late 1800s and peaked in the 1950s-70s (40 to 25cm) before declining  
521 over recent decades, consistent with the  $^{210}\text{Pb}$  based age model. The occurrence of  $^{137}\text{Cs}$  in the top ~40cm of the  
522 core is also consistent with the  $^{210}\text{Pb}$  based age of ~1950 at 40cm. Age uncertainty ( $1\sigma$ ) for the last 60 years of  
523 the core is estimated at  $\pm 2-3$  years. Note, sediment core top is at 3cm depth in core-liner.

524  
525



526  
527

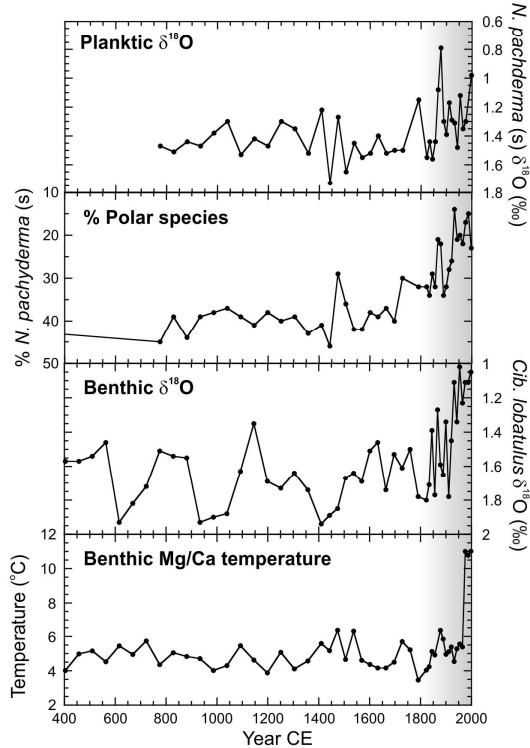
528 **Extended Data Figure 2. Age models for additional cores. a,**  $^{14}\text{C}$  age model based on linear interpolation of  
 529  $^{14}\text{C}$  dated planktic foraminifera (with  $1\sigma$  ranges) in sediment core KNR-178-48JPC (used for the DWBC<sub>LSW</sub> SS  
 530 reconstruction); yielding a modern core top age and average sedimentation rate of  $\sim 50\text{cm/kyr}$ . Note, core top is  
 531 at 3cm depth in core-liner. Insert shows the SCP profile for 48JPC based on the  $^{14}\text{C}$  age model, confirming the  
 532 modern age of the top sediments, with SCPs showing the expected profile: increasing from the late 1800s  
 533 onwards, peaking  $\sim 1950-1970$  and then declining afterwards. **b,** Updated age model for KNR-158-10MC (after  
 534 ref. <sup>47</sup>; used in Extended Data Fig. 1, examining regional near surface temperature trends in the NW Atlantic  
 535 during the Industrial era) using new  $^{210}\text{Pb}$  dating (CIC method) for the top 7cm and rejecting the anomalously  
 536 old  $^{14}\text{C}$  age at 4cm depth. A single detectable occurrence of  $^{137}\text{Cs}$  at 2-2.5cm (equivalent to 1957 on the  $^{210}\text{Pb}$   
 537 based age model) can be linked to the bomb peak at 1963, supporting the age model. Also note, SCPs were  
 538 found in the top 5cm of this core, confirming the Industrial era age for the top 5cm, however the low  
 539 concentrations prevent meaningful interpretation of the down-core trends and are not shown. **c,** Age model for  
 540 core OCE-326-MC29B (used for Tsub reconstruction of the NW Atlantic shelf).  $^{14}\text{C}$  ages of planktic  
 541 foraminifera (with  $1\sigma$  ranges) from ref. <sup>48</sup>. Support for this age model is provided by the SCP concentrations  
 542 (this study) which show the expected down-core profile<sup>39</sup> when plotted using the  $^{14}\text{C}$  ages.  $^{210}\text{Pb}$  dating<sup>48</sup> also  
 543 suggests a sedimentation rate of  $\sim 120\text{cm/kyr}$  for uppermost sediments, consistent with the  $^{14}\text{C}$  ages and SCP  
 544 profile.

545  
546

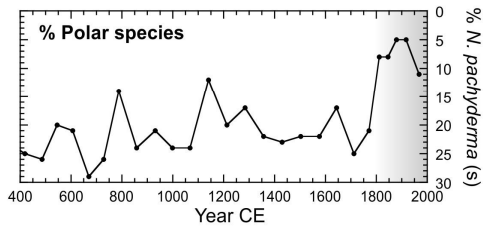
NW ATLANTIC SLOPE

NE ATLANTIC SPG

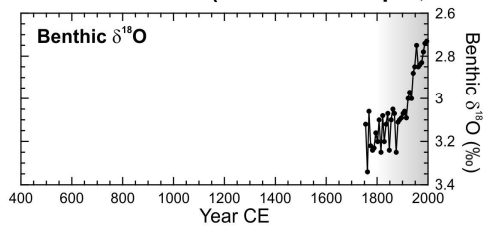
**a Emerald Basin (29MC, 250m water depth, site 2)**



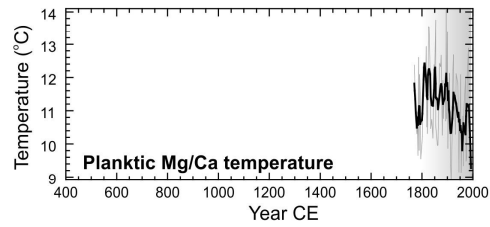
**b Laurentian Fan (13MC, site 3)**



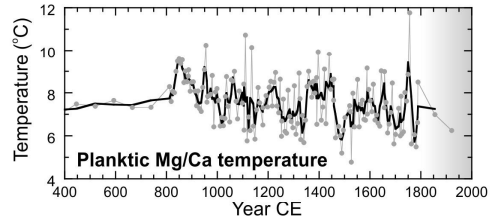
**c Gulf of St Lawrence (409m water depth, site 1)**



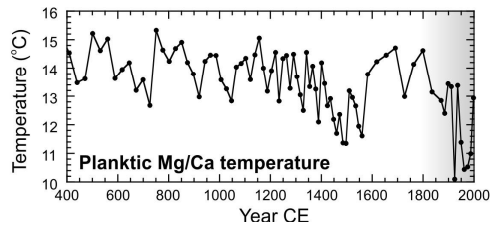
**d Gardar drift (site 4)**



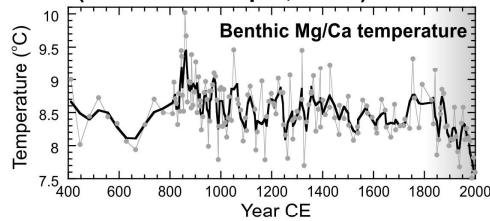
**e Bjorn drift (site 5)**



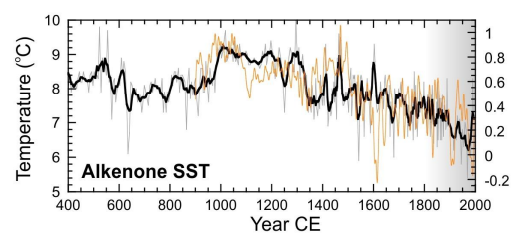
**f Feni drift (site 6)**



**g ENACW, formed in eastern SPG (899m water depth, site 7)**



**h \*North Iceland shelf/Rahmstorf SPG SST**



547

548

549

550

551

552

553

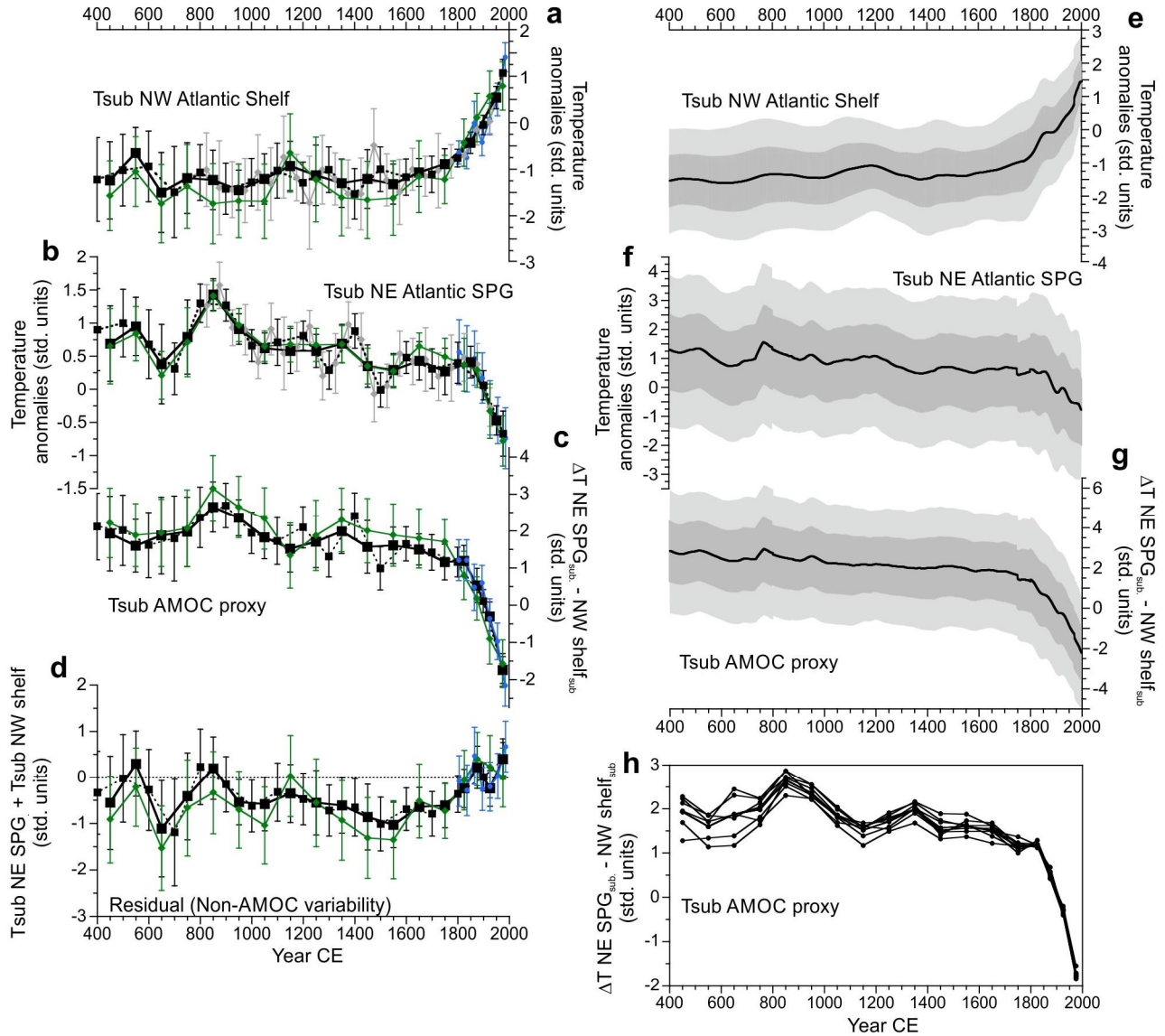
554

555

556

557

**Extended Data Figure 3. Raw data for construction of Tsub AMOC proxy shown in Fig. 3.** Locations are shown in Fig. 2b. **a-c**, Temperature proxy records from refs<sup>48-50</sup> used for the Northwest Atlantic stack, where model studies<sup>11,12</sup> indicate AMOC weakening results in warming of the surface and subsurface waters. **d-g**, records used to reconstruct Northeast Atlantic subpolar gyre subsurface temperatures: **d**, Gardar drift<sup>51</sup>, **e**, combined South Iceland data<sup>52,53</sup>, **f**, Feni drift<sup>54</sup>, **g**, Eastern North Atlantic Central Water (ENACW) largely composed of waters formed in the eastern SPG<sup>55,56</sup>, **h**, The high resolution alkenone SST record from the North Iceland shelf<sup>57</sup> was not included because it is not located within the open North Atlantic subpolar gyre, although it does also show the lowest temperature of the last 1600 years occurred during the most recent century, similar to the other Northeast Atlantic records. Also shown for reference is the Rahmstorf central subpolar gyre SST reconstruction (largely based on terrestrial proxies)<sup>6</sup>.



559

560

**Extended Data Figure 4. Different binning and averaging approaches and the residual temperature signal.**

561

**a & b**, Stacked, normalized proxy temperature data from the NW Atlantic shelf/slope (**a**) and NE Atlantic SPG

562

(**b**). **c**, The derived Tsub AMOC proxy calculated as the numerical difference between the stacks shown in **a** and

563

**b**. **d**, The residual temperature variability in stacks **a** and **b** not described by the (anti-phased dipole) Tsub

564

AMOC proxy shown in **c**, i.e. the in-phase temperature variability common to both stacks, calculated as the

565

numerical sum of the two stacks (if divided by two, this would be the numerical mean). This represents the

566

inferred non-AMOC related temperature variability common to both regions, and broadly resembles northern

567

hemisphere temperature reconstructions, most notably colder residual temperatures during the LIA, ~1350-1850.

568

For plots **a-d**: black solid line and squares, preferred binning (50yr for 1800-2000, 100yr for 400-1800); green

569

line and symbols, as for preferred binning but stacks are produced by first binning the proxy data at each site and

570

then averaging these binned site values, as opposed to binning all the proxy data together in one step (the former

571

ensures equal weighting for each site, the latter biases the final result to the higher resolution records); black

572

dashed line and symbols, 100yr bins offset by 50yr from the preferred bins; grey line and symbols, 50yr bins

573

(not shown for **c** and **d**); blue line and symbols; 30yr bins for 1790-2000. Error bars for **a-d** are  $\pm 2S.E.$  **e-g**, as for

574

**a-c** except using a Monte Carlo approach, using the published uncertainties for age assignment and temperature

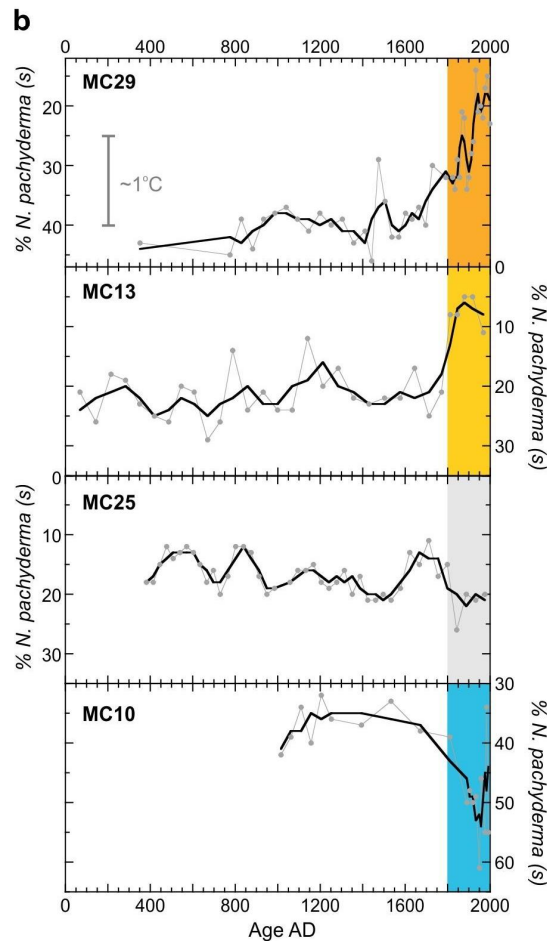
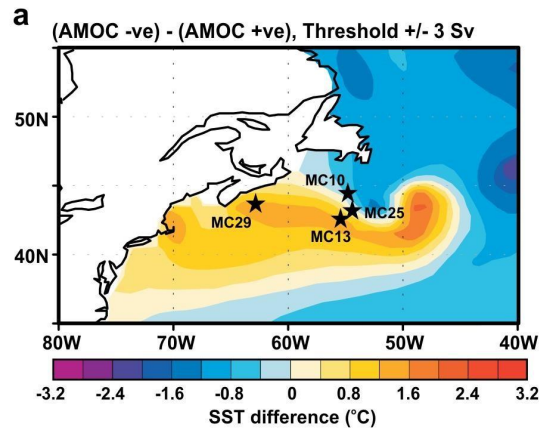
575

reconstructions; light and dark grey shading are  $\pm 1\sigma$  and  $\pm 2\sigma$ . **h**, Jackknife approach version of **c**, with each line

576

representing the Tsub AMOC proxy but leaving out one of the individual proxy records each time.

577



578

579

580

581

582

583

584

585

586

587

588

589

590

**Extended Data Figure 5. SST temperature response of the Northwest Atlantic to AMOC weakening. a,**

Modelled SST difference between weak and strong AMOC<sup>58</sup>. This pattern is model-dependent, with the study

cited here chosen because of its good agreement with observations of Gulf Stream variability<sup>58</sup>. Core locations

for **b** are shown by black stars. **b,** The percentage abundance of the polar species, *N. pachyderma* (sinistral), in

marine sediment cores from the Northwest Atlantic, as an indicator of near-surface (~75m) temperatures: a 15%

increase indicates ~ 1°C of cooling (note the reversed y-axes). The opposing trends over the last 200 years are

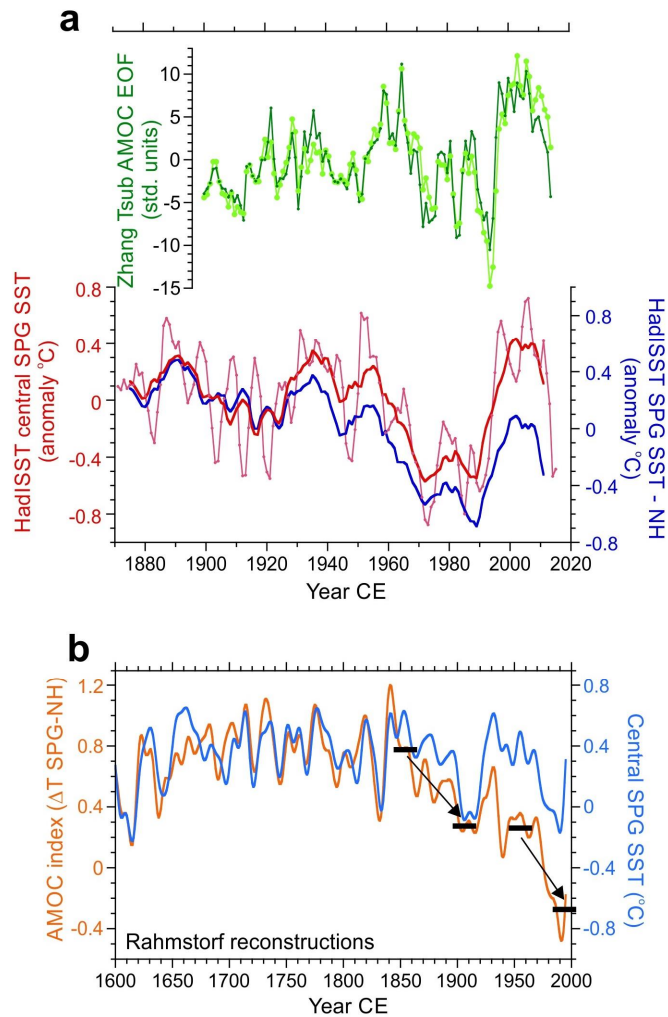
consistent with the modelled SST pattern for a weakening of the AMOC, as shown in **a**. Data and age models for

the cores are: OCE326-MC29, ref.<sup>48</sup>, using the original <sup>14</sup>C dating and as shown in Extended Data Fig. 2;

OCE326-MC13 and OCE326-MC25, ref.<sup>49</sup>, using the original <sup>14</sup>C age ties at the top and bottom of the core and

scaling the intervening sedimentation rate to the %CaCO<sub>3</sub> content<sup>49,59,60</sup>; KNR158-MC10 from this study and age

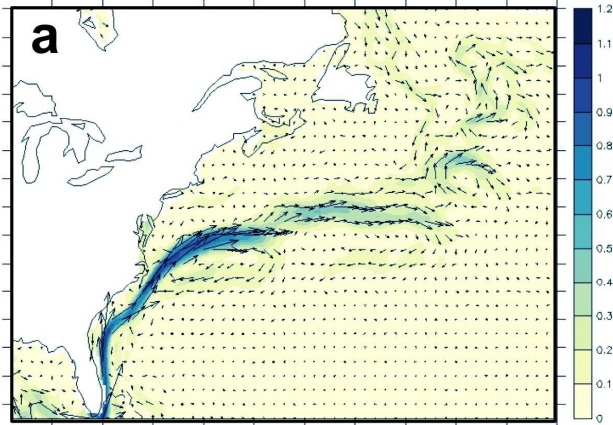
model presented in Extended Data Fig. 2.



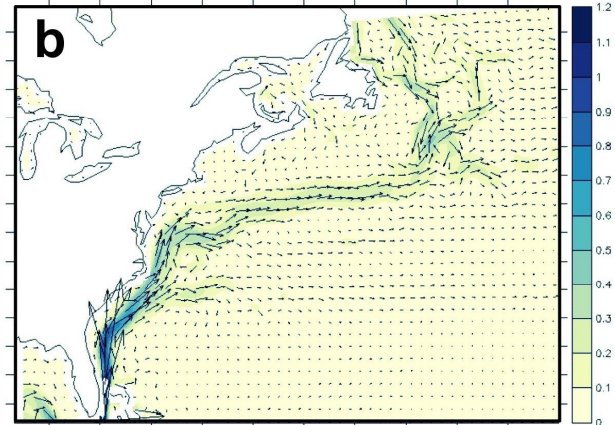
591  
 592  
 593  
 594  
 595  
 596  
 597  
 598  
 599  
 600  
 601  
 602  
 603  
 604  
 605  
 606  
 607  
 608  
 609  
 610

**Extended Data Figure 6. Temperature fingerprints of AMOC over the twentieth century.** **a**, Top, the Tsub AMOC fingerprint<sup>11</sup> using the EN4 dataset (light green is EOF1 of 1993-2003, as defined by Zhang<sup>11</sup>, applied to the EN4 data; dark green is the 2<sup>nd</sup> EOF of the North Atlantic) - no 20<sup>th</sup> century AMOC decline is shown by this observational based reconstruction; bottom, instrumental based reanalysis of the cold blob central SPG region (red, 3 yr and 11 yr smooth; 47-57N, 30-45W) used in the Rahmstorf SST AMOC proxy<sup>6</sup>. The reconstructed central SPG SST bears some resemblance to the Tsub AMOC fingerprint record, which is not unexpected since the central SPG forms a significant spatial component of the Tsub fingerprint. No clear decrease is shown by the central SPG SST, and the equivalent Rahmstorf AMOC proxy<sup>6</sup> (blue; central SPG  $\delta$  northern hemisphere (NH) temperature) declines through the twentieth century only due to the subtraction of the NH warming trend. **b**, Reconstructed (predominantly terrestrial-based proxy network) AMOC proxy (temperature difference between the central SPG and the NH; orange) and the central SPG SST reconstruction<sup>6</sup> (blue). As for the instrumental data shown in (a), the decline in the Rahmstorf AMOC index throughout the twentieth century is caused by the subtraction of the NH warming trend. There is a two-step decline in the AMOC proxy, at 1850-1900 and 1950-2000, the former mainly being the result of a strong cooling of the SPG (likely weakening northward heat transport, paralleling the weakening shown by our DWBC proxy), whereas the late twentieth century decline was mainly due to the subtraction of the strong NH warming trend, rather than a persistent cooling of the SPG.

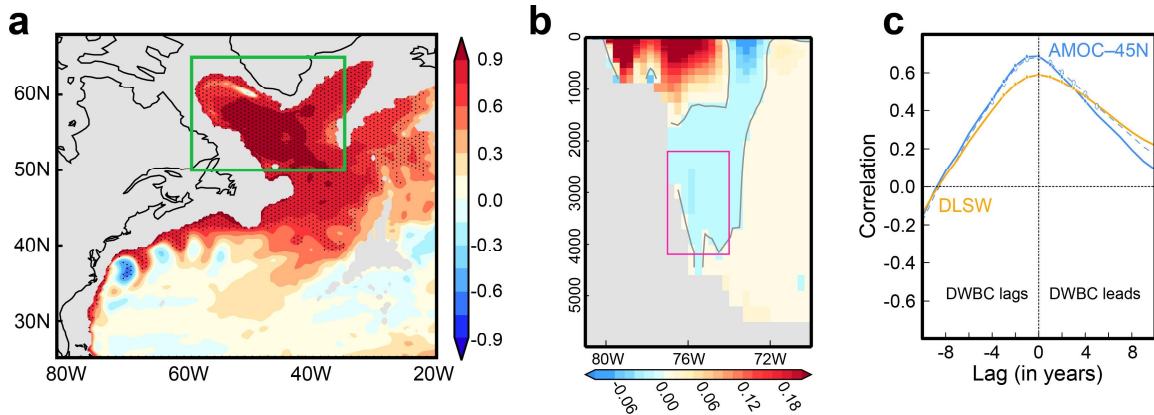
GC2 climatological Surface Currents



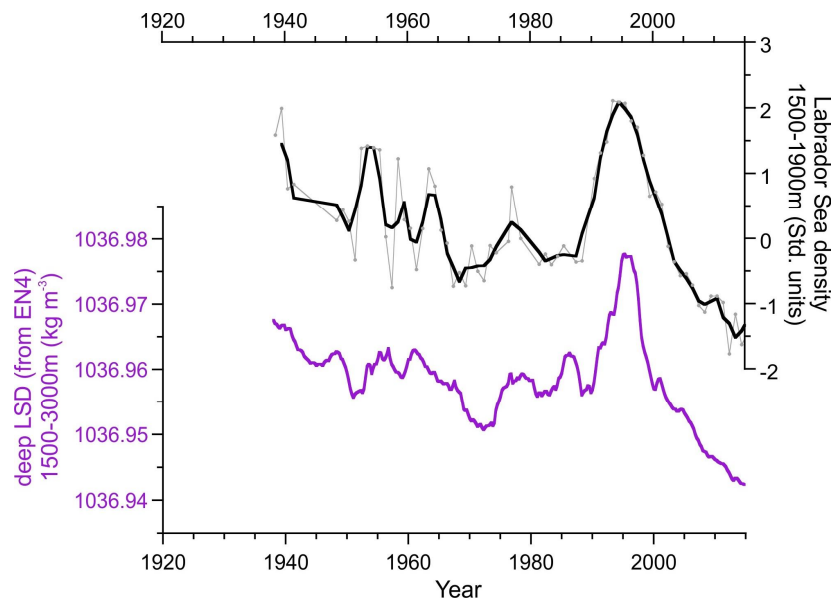
Observed (OSCAR) Surface Currents



611  
612 **Extended Data Figure 7. DWBC changes in model HadGEM3-GC2. a,b** Climatological surface current  
613 direction (in arrows) and speed (shaded, m/s) in the control simulation with HadGEM3-GC2 and the satellite  
614 product OSCAR, respectively.  
615  
616  
617

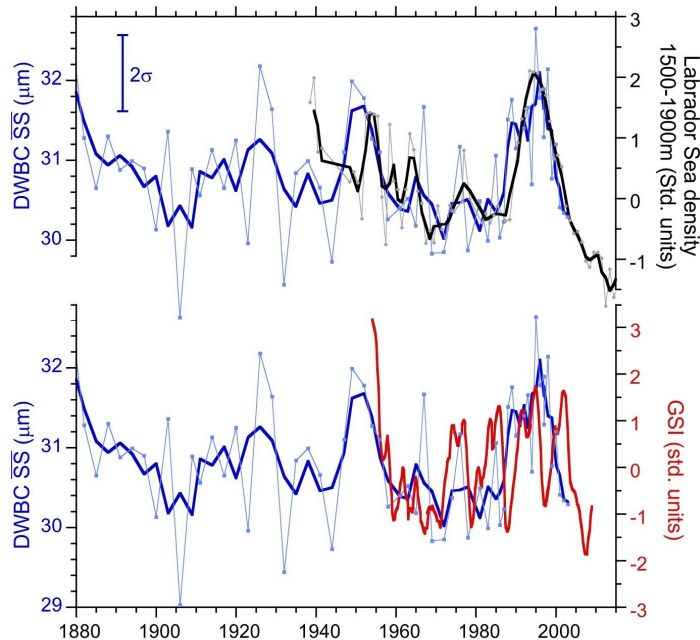


618  
619 **Extended Data Figure 8. The modelled link of DWBC velocity with deep Labrador Sea density and**  
620 **AMOC in the HiGEM model. a,** Correlation of the vertically-averaged ocean density (1000-2500m) with deep  
621 Labrador Sea density index (dLSD as defined by ref. 4; green box, 1000-2500m average) in a 340 year present  
622 day control run of the HiGEM model (see ref 36). **b,** Climatology of the modelled meridional ocean velocity  
623 ( $\text{ms}^{-1}$ ) averaged between 30-35°N, illustrating the modelled position of the DWBC **c,** Cross-correlations between  
624 modelled averaged DWBC flow speed in pink box in **b** and indices of dLSD and AMOC at 45°N (dashed line is  
625 without the Ekman component). Note that the box over which the DWBC flow index in **c** is averaged has  
626 changed with respect to Fig. 1 in the main paper in order to take into account of the fact that the return flow is  
627 deeper in HiGEM than in HadGEM3-GC2.  
628  
629



630  
631  
632  
633  
634  
635  
636  
637  
638  
639  
640

**Extended Data Figure 9. Comparison of Labrador Sea density parameters.** The model-based deep Labrador Sea density (dLSD) parameter, proposed by ref. 4, using the EN4 reanalysis dataset, incorporates a larger area and greater depth range than instrumental data-only studies such as ref. 5, which examines past variability in Labrador Sea convection and focuses on the central Labrador Sea and depths <2000m region, where most observational data is available. The comparison, here, of dLSD (purple line, 3 yr mean) using the EN4 dataset with instrumental data of density changes in the central Labrador Sea at 1500-1900m depth (black line, annual averages and 3 yr mean) illustrates that the two parameters show very similar variability, both being dominated by the density changes caused by deep convection in the Labrador Sea, which can reach down to ~2000m. Estimates of uncertainty are discussed in ref. <sup>61</sup>.



641  
642  
643  
644  
645  
646  
647

**Extended Data Figure 10. Comparison with Gulf Stream Index (GSI).** The direct influence of the changing position of the Gulf Stream on the grain size of our core sites can be ruled out through comparison of instrumental records of the Gulf Stream position (the GSI, from ref. <sup>58</sup>) with the down-core data in 56JPC. No clear correlation is observed between the GSI and our SS mean grain size data in core 56JPC, contrasting with the coupling between our SS data (inferred DWBC<sub>LSW</sub> flow speed) and density changes in the deep Labrador Sea.  $2\sigma$  SS error bar ( $n=30$ ) is for 3-point mean (bold).